The Case Study for Evaluation of Landslides Volume and Moving Paths of Single Falling Rock

Feng-Chi Huang[a] Yi-Hsuan Lee[a] Jiun-Ting Lin[b] Kuo-Wei Chen[a] Chen-Yu Chen[a] Kuo-Lung Wang[b]

[a] Research Technology Development Team, Soil and Water Conservation Bureau Council of Agriculture, Executive Yuan, Taiwan (R.O.C)
[b]Department of Civil Engineering, University of National Chi Nan, Taiwan (R.O.C)
E-mail: fchuang@mail.swcb.gov.tw, limermaidyam@gail.com, nokilin@gmail.com, ckw@mail.swcb.gov.tw, cychen59@gmail.com, kuolung@gmail.com

Abstract –

Landslides are natural evolution of topography. Since human behavior started reaching to mountain area, landslide disasters often occur and threaten people. The study uses the case of typhoon-Meranti-induced Hongye landslide in Taiwan on September 15th, 2016 to determine the landslide terrain feature, geological conditions, and disaster impact area by surveying the site for investigate and using the unmanned aerial vehicle (UAV) for monitoring. The UAV's aerial photos are used to build the 3D model, orthophoto and digital surface model (DSM). The landslide area can be drawn with the area orthophoto. Compare the digital terrain model before and after the landslide to evaluate the terrain change of slope and landslide volume. While surveying the site of Hongye landslide, we found there is a risk of rock fall. To assess the motion track and form of the rock on slope, this study uses RocScience Rocfall 5.0 to conduct stability analysis to analyze the potential path and risk of the rock.

Keywords –

UAV; DTM; Landslide volume evaluate; RocScience

1 Introduction

Landslides are important type of natural disaster worldwide, and can cause major hazard in mountain area, costing human casualties and economic losses. Landslides can be triggered by intense rainfall, earthquakes or human activities. Take rainfall-induced landslide as example, a landslide dam was formed in Taiwan by 0610 heavy rainfall event, and was just collapsed few hours later (Kuo-Lung Wang et al., 2016) ; In Brazil, heavy thunderstorms occurred and triggered thousands of landslides on steep slopes with trees and block rich debris materials converged into the river channels, hence avalanches down valley (André S. Avelar et al., 2013). To avoid human casualties and economic losses, there is a mission not only to understand the landslide process but also the landslide-triggered mechanisms. Analysis of historical records of landslide and reliable monitoring methods seems important.

The use of remote-sensing technology for mapping and monitoring landslide has improved a lot since the last decade, including the (airborne or terrestrial) laser scanning or unmanned aerial vehicles (UAV). This paper focuses on the research of UAVs landslide monitor, analysis and application. Unmanned Aerial Vehicles (UAVs) are an inexpensive, low- labor costs, effective, user-friendly and new remote sensing tool (Mark A. Fonstad et al.,2013； J. Travelletti et al.,2012； M.J. Westoby et al.,2012), which can acquire high resolution spatial data. (Darren Turner et al., 2012； Mark A. Fonstad et al., 2013). Development of UAV platforms requires broad technical skills covering platform development, data post-processing, and image analysis (Joshua Kelcey et al., 2012). Therefore, Structure from Motion (SfM) computer vision techniques were applied to derive ultra-high resolution 3D models from multi-view aerial photography (Arko Lucieera et al., 2014). SfM is a flexible approach to capturing complex topography (M.J. Westoby et al., 2012). Then, the imagery can be used to produce dense point clouds using multi-view stereopsis techniques (MVS) combining computer vision and photogrammetry (Steve Harwin et al., 2012). Therefore, UAV application is a capability of producing 3D model, orthophoto and digital terrain model (DTM). Furthermore, comparing a laser scanner survey of the same site, SfM-MVS produced comparable data and reduced data collection time by 80% (M. R. James et al., 2012).

UAVs are ideal tools to map and monitor features at the Earth surface. For instance, chalk sea cliffs in UK (John Barlow et al., 2017) ; Italy mapping discontinuities within a marble quarry (Riccardo Salvini

et al., 2016) ; changing snow and polar vegetation of Antarctic moss beds (Arko Lucieera et al., 2014), etc. Now, UAVs have been used to monitor landslides (Kuo-Lung Wang et al., 2016; U. Niethammer et al., 2012 ; Arko Lucieer et al., 2014). UAV ' s aerial photos can be used to produce a high-resolution ortho-mosaic of the entire landslide, 3D models and digital terrain models (DTMs) of several regions, that more geological formation can be discovered from (Kuo-Lung Wang et al.,2016; U. Niethammer et al.,2012; Mariella Danzi et al.,2012). An environmental remote sensing application using a UAV is specifically aimed to reducing the data gap between field scale and satellite scale in soil erosion monitoring (Sebastiand' Oleire-Oltmanns et al., 2012).

High resolution digital terrain models produced by UAV' s collected data should be based on the real-world and accuracy coordinate system in order to measure distance, observe elevation changing or analysis slope. However, Khairul has evaluated the accuracy of slope mapping results from different altitudes at semi-undulated area and undulated area and found altitudes did have an influence on the slope accuracy (Khairul Nizam Tahar, 2015). Therefore, during the process producing digital terrain models, the point clouds are in an arbitrary coordinate system and need to be georeferenced. The point clouds are transformed into a real-world coordinate system using either a direct georeferencing technique that uses estimated camera positions (the UAV's log file) or via a Ground Control Point (GCP) technique that uses automatically identified GCPs within the point cloud (Sebastiand'Oleire-Oltmanns et al., 2012 ; Darren Turner et al., 2012; Mark A. Fonstad et al., 2013; SteveHarwin et al., 2012). The models fitted the ground control network are able be within a standard error with horizontal and vertical precision in the centimeter range (John Barlow et al., 2016; Mark A. Fonstad et al., 2013).

The UAV has demonstrated its capability for producing valuable landslide data, imaging fissures and displacements on the landslide surface (U. Niethammer et al., 2012). Also, UAV can evaluate landslide failure volume through volumetric analysis, a comparison of sequential models (John Barlow et al., 2016).

Data capture through UAV photogrammetry can provide useful terrain information, including slope condition, discontinuities, slope geometry or unattainable measurements, for slope numerical modeling of stability or kinematic analysis (Riccardo Salvini et al., 2016 ; John Barlow et al., 2017 ; Mariella Danzi et al., 2012 ; Kuo-Lung Wang et al.,2016). Cross sections and joint system data were obtained from DTM and used as input parameters for the slope stability analyses (Á kos Török et al., 2017). For instance, John Barlow used the method to analyze over sea cliffs and coast (John Barlow et al., 2017); Á kos Török modelled the rocky slope by 2D FEM (Finite Element Method) software and identified potential hazards such as planar failure, wedge failure and toppling (Á kos Török et al., 2017). By geological analysis and correlation between soil properties and geotechnical behavior can explain the catastrophic slope movement mechanisms and processes (André S. Avelar et al., 2013).

2 Research Preparation

2.1 Geological setting

The landslide located only 4.3 km away from the Luye fault, which is a north-south directional reverse fault. The region geological, aged about Eocene or earlier, is Pilushan Formotion (Ep). The main lithology is Slate and Phyllite, but in the layer there is the thicker Meta-Sandstone layer, including Calcareous, Arkose (Figure 1). On September 15th, 2016, typhoon Meranti occurred, with the rainfall of 513.5mm accumulated rain and 19mm/hr rainfall intensity, inducing the first landslide that ranged about 5.62 hectares.

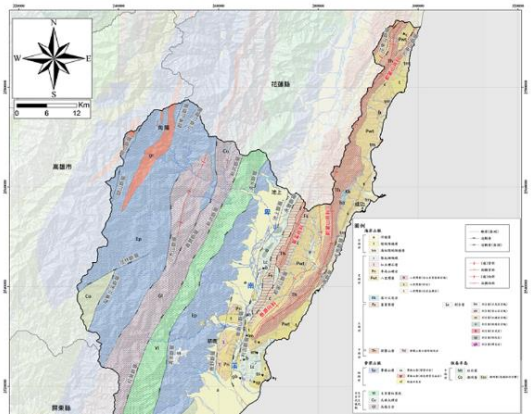

Figure 1. The regional geological map in the research case

2.2 Numerical Model Analysis

2.2.1 Soil material

Marinos presents a quick and easy method to estimate the engineering parameters of rock mass (Marinos and Hoek, 2000). This method considers three main parameters as follows: the uniaxial compressive strength (σ_{ci}), a material constant (m_i) related to the frictional properties of the rock, and the Geological Strength Index (GSI) that response to the geological joint condition of rock. The two constant, (σ_{ci}) and (m_i), can be obtained from laboratory test, but both of the

value still can be estimated if there is no test data. Then, the engineering parameters of rock, including friction angle (φ) and cohesive strength (c) can be determined with Figure 2 and Figure 3 according to the estimated value. This study assesses the corresponding parameters of the above description, shown in Table 1.

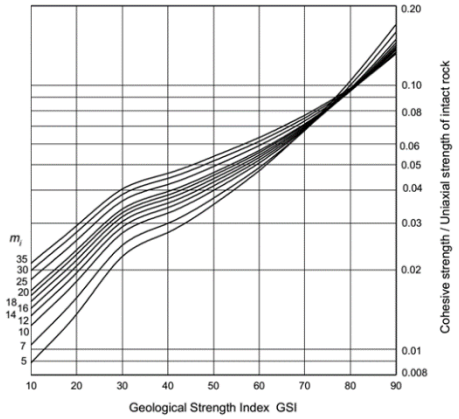

Figure2 Relationship between ratio of cohesive strength to uniaxial compressive strength of intact rock (c/σ_{ci}) and GSI for different (m_i) values (Marinos and Hoek,2000)

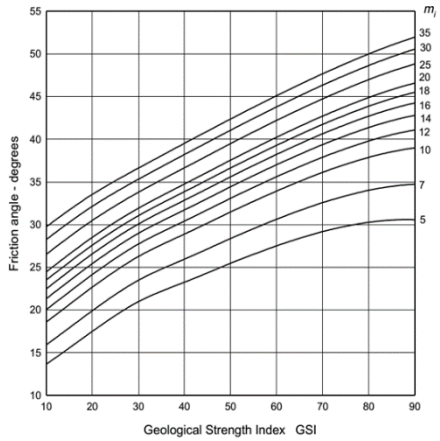

Figure3 Friction angle φ for different GSI and mi values(Marinos and Hoek,2000)

Table1 Field estimates of rock mass properties by Marinos and Hoek,2000

Grade	Uniaxial Comp. Strength (σ_{ci}) MPa	Values of the constant (m_i)	Geological strength index (GSI)	Cohesive strength / Uniaxial etrength of intact rock (c/σ_{ci})	Cohesive strength (C) KPa	Friction angle (φ°)
R1	1-5	7-11	10-15	0.011-0.015	11-15	17-21

2.2.2 Rockfall Model

This study adopts the rockfall analysis in RocScience Rocfall 5.0.This statistical analysis program can assess the energy, velocity, bounce-height and location of rock endpoints of the process of motion rock over the slope, and uses the Monte Carlo techniques to do the risk level statistics. This program needs to be defined with the slope and the rock geometry and material properties, including dynamic friction, rolling friction coefficient, rock density, rock mass and the slope terrain elevation and so on.

3 Research procedures

3.1 Landslide terrain change and volume evaluate

3.1.1 Aerial survey mission and 3D model

This study uses remote-controlled UAV Phantom 3 Professional equipped with digital camera and GPS to acquire airborne digital photographs on September 16, 2016 and March 24, 2017. The images recorded in 2016 is in emergency mission, the image resolution ranges between 0.042m to 0.370m, and did not set the ground control point. UAV mission in 2017 took different elevation as Aerial survey route (Figure 4) to raise the image resolution which ranges between 0.036m to 0.190m, and 10 ground control points were set around the landslide area to calibrate the elevation (Figure 5).

This study uses Bentley Context Capture version 4.0 to feature the points of the aerial photos by aerotriangulation and produce the three-dimensional model. The 2016 and 2017 orthophoto and the digital surface model (DSM) were also be obtained. The DSM grid size is 0.140m of 2016 and 0.093m of 2017.

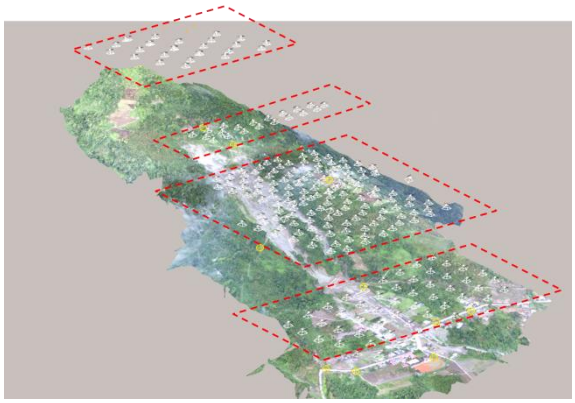

Figure 4 UAV aerial survey route

Figure 5 Ground control points

3.1.2 Terrain change tracking and volume evaluation

This study uses the orthophotos made from aerial images after the landslide to plot the range of the exposed and landslide area. Aerial survey had done again in the following year to track the changes of the landslide area. Comparing orthophotos between 2016 and 2017 can find that the part of the vegetation in the landslide area has been recovered, but the upper edge of the landslide seems to be expanded, and the new tension cracks can be discovered (Figure 6).

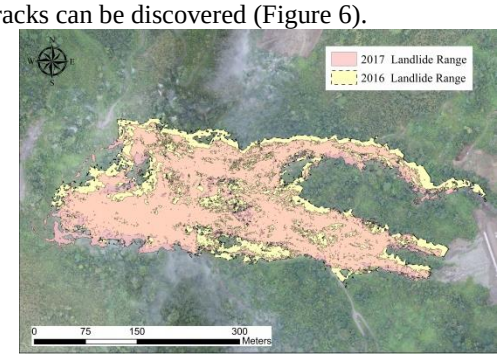

Figure 6 Orthophotos comparison between 2016 and 2017

This study compares the DSM before and after the landslide, determines the elevation difference after landslide and evaluates the landslide volume. The results show that the landslide area is about 56,194 m^2, and the mean elevation difference of the landslide area is 2.70 m, including the deepest erosion of 13.48 m and the highest accumulation of 21.25m (Figure 7). The landslide area is divided 56,194 grids of single 1m^2, including 14,609m^2 of the accumulation area, 41,585m^2 of the erosion area that defined as five levels according to the erosion depth (Table 2). After the statistics of the landslide erosion area, the landslide volume 211,466 m^3 is evaluated.

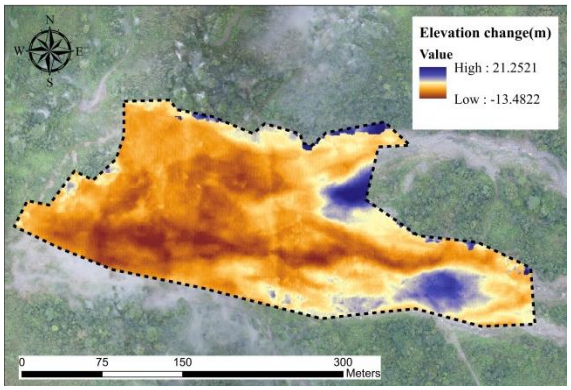

Figure 7 Terrain change after landslide

Table 2 Landslide area for five levels according to erosion depth

Depth(m)	Number of Grid (m^2)
0~2.5	9415
2.5~5.0	12175
5.0~7.5	10715
7.5~10	7316
10~13.48	1964

3.2 Numerical Analysis of Rockfall

3.2.1 Material parameters and analysis assumptions

According to the surface model of 2017, the risk of dangerous rock of the landslide is estimated. The length, width and height of the rock is 9.20m, 5.70m and 3.60m respectively. The rock volume is about 65.22m^3. Through the investigation, the rock is considered as the sandstone with unit weight of 2.70 (T / m^3), and the rock is about 176,094 kg. In addition, the surface of the slope after the landslide is extremely weathering erosion, assessed the friction angle of the slope is 21 °. This study assumes the rock is moved by the influence of the foundation loss and earthquake.

According to the terrain slope and the shadow map, the four tracks of the motion rock are decided (Fig. 8), and the rock is located on intersection points of each path. Two erosion depth : 3.60m (rock height) and 13.48 m (maximum erosion depth) were analyzed and also the seismic acceleration 400 gal. Considered the possible aggravation, every condition of the analysis tests 100 times, and statistics of the end location and the probability of occurrence.

Table 3 Surface-erosion impact rock stability anlyisis

track	Rock displacement and occurrence probability					Highest probability and Rock displacement	
	Erosion Depth	Max Displacement(m) **(A)**	Percentage (%)	Min Displacement (m)	Percentage (%)	Percentage (%)	Highest probability displacement (m) **(B)**
1	3.6	47.09	100	-	-	100	47.09
	13.48	110.49	1	47.09	87	87	47.09
2	3.6	54.52	100	-	-	100	54.52
	13.48	81.78	1	54.52	96	96	54.52
3	3.6	58.53	83	45.91	17	83	58.53
	13.48	109.02	1	45.91	21	74	58.53
4	3.6	51.08	100	-	-	100	51.08
	13.48	51.08	100	-	-	100	51.08

Table 4 The earthquake-acceleration impact rock stability anlyisis

track	Rock displacement and occurrence probability					Highest probability and Rock displacement	
	Erosion Depth	Max Displacement(m) **(C)**	Percentage (%)	Min Displacement (m)	Percentage (%)	Percentage (%)	Highest probability displacement (m) **(D)**
1	0	47.09	100	-	-	100	47.09
	3.6	82.31	1	47.09	93	93	47.09
	13.48	138.66	1	47.09	86	86	47.09
2	0	54.52	100	-	-	100	54.52
	3.6	209.02	1	54.52	98	98	54.52
	13.48	336.26	1	54.52	72	72	54.52
3	0	58.53	85	15	45.91	85	58.53
	3.6	109.02	1	45.91	17	75	58.53
	13.48	109.02	5	45.91	12	33	58.53
4	0	51.0	100	-	-	100	51.0
	3.6	68.29	1	51.08	95	95	51.08
	13.48	68.29	2	51.08	95	95	51.08

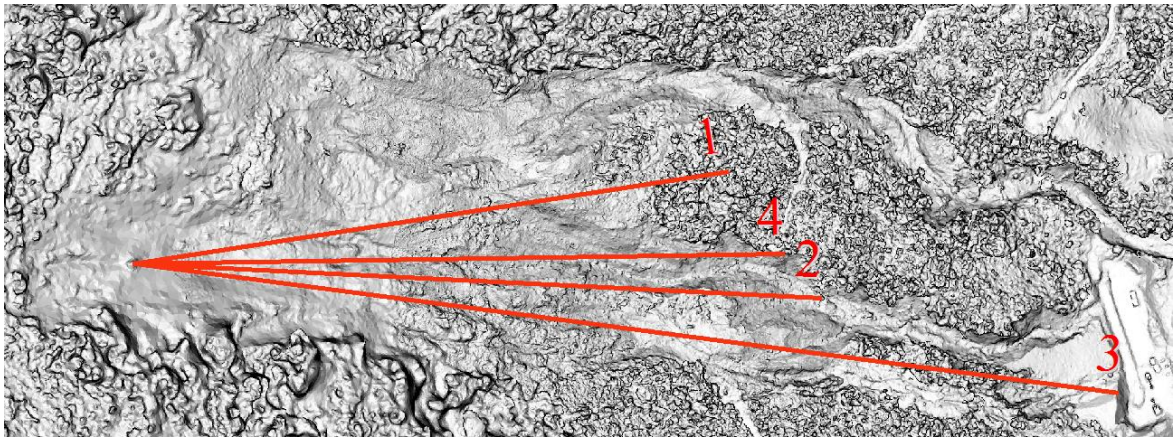

Figure 8 Moving paths of single falling rock

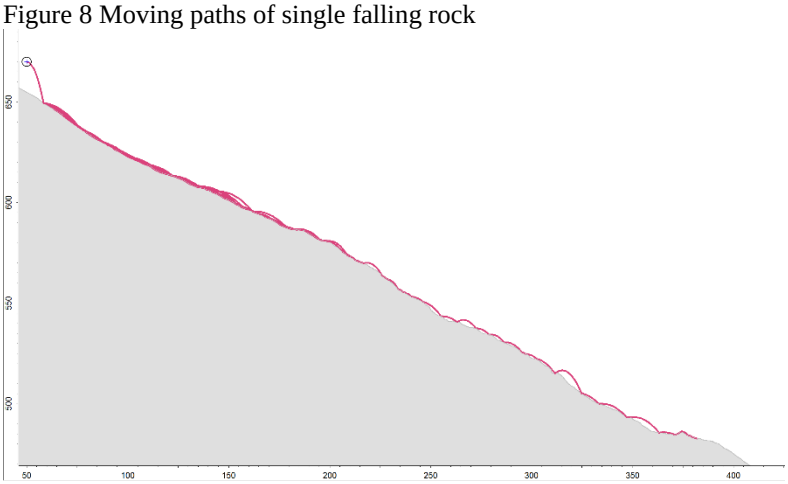

Figure 9 Moving path of track 2

3.2.2 Results and discussion

According to the results, this study shows that with only the terrain erosion without earthquake impact; the rock lost support would fall and slide (Table 3). Erosion of depth 3.60m, the motion of the displacement the value A and B seems the same. Erosion of depth 13.48m, the motion paths are almost the same except for track 4, which the maximum probability of occurrence and the maximum displacement distance is not the same. Considering the acceleration of earthquake, the value C and D are the same of the nonerosion slope.

In addition, when the slope occurs erosion, the probability of maximum displacement and the highest occurrence for each erosion depth are different (Table 4). The path 2 in the erosion depth of 13.48m, the displacement of the rock is 336.26m, which is the maximum displacement of all paths . The track of path 2 may have the factors of terrain that leads the rock to the bounce, nonstop at the gentle area and keeps moving on. So, this path is the highest risky path of all (Figure 9).

4 Conclusions

1.Using UAV to record images for a wide-range area tracking and ground control points improves the measurement accuracy. The details of the landslide region can be presented more accurate, such as this study survey investigate found that above the original landslide exists the tension cracks, and scope of the landslide tend to be expanded.

2. Using the orthophoto to plot the range of landslide which is considered as a basis for the terrain surface elevation difference comparison of before and after the landslide, the surface elevation difference is the landslide volume. The concept of this calculus is that when the landslide happens, the surface of the area is exposed without vegetation, so the digital surface model elevation of the area is equal to the digital terrain model, therefore, it presents the exact terrain elevation, and the comparison between the pre-disaster (DEM) and after-disaster (DSM) of the landslide area elevation is determined.

3.This study uses the numerical analysis program RocFall to conduct the rock motion track analysis.

According to the gradient of the slope, 4 possible motion paths are predicted and of which two factors of the loss of the foundation support and the earthquake effect are assumed. The rockfall stability analysis is carried out to evaluate the fall end of each path and the probability of occurrence and to presume the most possible occurrence and damage possible rock motion path.

5 References

[1] Á kos Török, Á rpád Barsi, Gyula Bögöly, Tamás Lovas, Á rpád Somogyi and Péter Görög. Slope stability and rock fall hazard assessment of volcanic tuffs using RPAS and TLS with 2D FEM slope modelling. Natural Hazards and Earth System Sciences :56-85, 2017.

[2] Avelar AS, Coelho Netto AL, Lacerda WA, et al. Mechanisms of the recent catastrophic landslides in the mountainous range of Rio de Janeiro, Brazil. In: Margottini C, Canuti P, and Sassa K (eds) Landslide Science and Practice. Volume 4: Global Environmental Change. Berlin: Springer, 265–270, 2013.

[3] d'Oleire-Oltmanns S, Marzolff I, Peter K, et al. Unmanned aerial vehicle (UAV) for monitoring soil erosion in Morocco. Remote Sensing 4: 3390–3416, 2012.

[4] Fonstad MA, Dietrich JT, Courville BC, et al. Topographic structure from motion: A new development in photogrammetric measurement. Earth Surface Processes and Landforms 38(4): 421–430, 2013.

[5] Guzzetti F, Mondini AC, Cardinali M, et al. Landslide inventory maps: New tools for an old problem. Earth-Science Reviews 112: 42–66, 2012.

[6] Harwin S and Lucieer A . Assessing the accuracy of georeferenced point clouds produced via multi-view stereopsis from unmanned aerial vehicle (UAV) imagery Remote Sensing 4: 1573–1599, 2012.

[7] James MR and Robson S Straightforward reconstruction of 3d surfaces and topography with a camera: Accuracy and geoscience application. Journal of Geophysical Research 117: F03017, 2012.

[8] John Barlow and Jamie Gilham. Stability analysis of chalk sea cliffs using UAV photogrammetry.19th EGU General Assembly, 2017.

[9] John Barlow, Jamie Gilham & Ignacio Ibarra Cofrã. Kinematic analysis of sea cliff stability using UAV photogrammetry. International Journal of Remote Sensing, 38:2464–2479, 2017.

[10] Kelcey J and Lucieer A. Sensor correction of a 6-band multispectral imaging sensor for UAV remote sensing. Remote Sensing 4: 1462–1493, 2012.

[11] Khairul Nizam Tahar. Multi rotor UAV at different altitudes for slope mapping studies. The International Archives of the Photogrammetry, Remote Sensing and Spatial Information Sciences, XL-1/W4, 2015.

[12] Kuo-Lung Wang and Zhi-Jie Huang. Discover failure mechanism of a landslide dam using UAV. Proceedings of the 16th International Conference on Computing in Civil and Building Engineering (ICCCBE 2016). MOST 103-2625-M-260-001, 2016.

[13] Lucieer A, Turner D, King DH, et al. Using an Unmanned Aerial Vehicle (UAV) to capture microtopography of Antarctic moss beds. International Journal of Applied Earth Observation and Geoinformation. 27 (Part A): 53–62, 2014.

[14] Marinos, P. and Hoek, E. GSI: A geologically friendly tool for rock mass strength estimation: Proceedings, GeoEng 2000, Melbourne, Australia, 2000.

[15] Mariella Danzi, Giuseppe Di Crescenzo, Massimo Ramondini & Antonio Santo. Use of unmanned aerial vehicles (UAVs) for photogrammetric surveys in rockfall instability studies. Società Geologica Italiana, 2012.

[16] Niethammer U, James MR, Rothmund S, et al. UAV-based remote sensing of the Super-Sauze landslide:Evaluation and results. Engineering Geology 128: 2–11, 2012.

[17] Riccardo Salvini, Giovanni Mastrorocco, Marcello Seddaiu, Damiano Rossi and Claudio Vanneschi. The use of an unmanned aerial vehicle for fracture mapping within a marble quarry Carrara Italy photogrammetry and discrete fracture network modelling. Geomatics, Natural Hazards and Risk, 2016.

[18] Travelletti J, Delacourt C, Allemand P, et al. Correlation of multi-temporal ground-based optical images for landslide monitoring: Application, potential and limitations. ISPRS Journal of Photogrammetry and Remote Sensing 70: 39–55, 2012.

[19] Turner D, Lucieer A and Watson C. An automated technique for generating georectified mosaics from ultra-high resolution Unmanned Aerial Vehicle (UAV) imagery, based on Structure from Motion (SfM) point clouds. Remote Sensing 4: 1392–1410, 2012.

[20] Westoby M, Brasington J, Glasser N, et al. 'structure- from-motion' photogrammetry: A low-cost, effective tool for geoscience applications. Geomorphology 179: 300–314, 2012.